Ultrafast Spectroscopy Reveals Slow Water Dynamics in Biocondensates

Keegan A. Lorenz-Ochoa and Carlos R. Baiz*

Department of Chemistry, University of Texas at Austin, Austin, TX 78712, USA

Email: cbaiz@cm.utexas.edu

Abstract

Cells achieve high spatiotemporal control over biochemical processes through compartmentalization to membrane-bound, as well as membraneless organelles that assemble by liquid-liquid phase separation. Characterizing the balance of forces within these environments is essential to understanding their stability and function, and water is an integral part of the condensate, playing a nontrivial role in mediating the electrostatic and hydrogen bonding interactions. Here we investigate the picosecond hydrogen-bond dynamics of a model biocondensate consisting of a peptide Poly-L-Arginine and the nucleic acid adenosine monophosphate (AMP) using ultrafast two-dimensional infrared (2D IR) spectroscopy. We investigate three vibrational modes, the arginine side chain C=N stretches, an AMP ring mode, and the amide backbone carbonyl stretches, to provide different perspectives. In general, dynamics slow down considerably between the dilute phase and the condensate phase for each vibrational probe. For example, the arginine side chain C=N modes slows from 0.38 ps to 2.26 ps due to strong electrostatic interactions. Hydrogen bond lifetime computed from all-atom molecular dynamics simulations provide an atomistic interpretation. Simulations predict that a significant fraction of water molecules are highly constrained within the condensate. We attribute this slowdown in dynamics to a highly disordered and extremely crowded water environment.

Introduction

Cells have evolved remarkable ways to achieve high spatiotemporal control over biological processes, by compartmentalizing biomolecules via membrane-encapsulated and membrane-less organelles, such as the nucleolus, Cajal bodies, or stress granules[1–3]. The importance of biomolecular condensates (BMCs) in mediating biological processes, including gene regulation, signaling, and storage/sequestration, highlights the critical need to understand fundamental biomolecular interactions in these complex multicomponent environments[2,4–6]. BMCs are complex systems consisting of a dense phase enriched in bio-polymers like protein, DNA, and RNA that remain separated from the cytosol environment[7,8]. These condensates form via liquid–liquid phase separation, a process stabilized by dipole–dipole, electrostatic, cation–pi, and pi–stacking interactions. Considering the complexity of the systems, investigating the relative strengths of these interactions and their role in driving liquid-liquid phase separation, or dictating the thermodynamic stabilities, has been challenging for modern experimental techniques[7,9–11].

Water constitutes about 70% of the condensate volume, and water molecules within the condensate either directly solvate the biomolecules or are confined to nanometer-scale pores and constrained by strong electrostatic interactions[12,13]. These ultra-crowded environments within the BMCs disrupt the long-range H-bond networks present in pure water and instead produce dynamics

significantly different from the bulk, analogous to the crowded environments in the cytosol[14,15]. Considering the importance of H-bonding in biological processes, it is essential to directly probe the local environments and dynamics within the condensate phase, understand the molecular-level structure, and elucidate interactions that lead to phase separation. From a biophysical perspective, it is important to understand the balance of thermodynamic driving forces that stabilize the condensate and the behavior of biomolecules within them[16–20].

Ultrafast two-dimensional infrared (2D IR) spectroscopy probes the time-evolving vibrational frequencies of the biomolecules. Frequency fluctuations are generally driven by the sub-picosecond H-bond rearrangements around biomolecules, thus reporting on the local H-bond environments[21–24]. Experimentally, 2D IR spectra are measured by applying a sequence of ultrafast mid-infrared laser pulses to excite and subsequently probe the vibrational modes of molecules. This technique has been used to elucidate dynamics in various biological systems, including proteins, nucleic acids, lipid membranes, and dynamics within crowded environments[25–31]. Recently, 2D IR spectroscopy has even been applied to study secondary structure formation within biomolecular condensates[32]. Proteins contain several vibrational modes that are highly sensitive to the local environments, such as the amide carbonyl stretching modes that provide a measure of secondary structure and solvent exposure of the protein backbone[33–35]. Here we used a model condensate consisting of linear Poly-L-Arginine (Poly-R) peptide combined with adenosine monophosphate (AMP), known to facilitate RNA partitioning, as shown in **Figure 1**[36]. This system contains the key interactions that stabilize bio-condensates, including strong electrostatic interactions, cation–pi, and H-bonding. The 2D IR measurements probe the picosecond dynamics of AMP ring modes, arginine C=N stretching modes, and the backbone amide I modes.

Results

Interpretation of FTIR Spectra.

Measured FTIR spectra of the individual components, AMP and Poly-R, as well as the condensate phase of the two combined, is shown in **Figure 1C**. In AMP, two narrow peaks corresponding to the adenosine ring modes are present at 1577 cm^{-1} and 1624 cm^{-1}. These ring modes arise from C-C and C=C stretching modes in addition to a pyrimidine ring mode[26]. In the Poly-R spectra, three peaks are observed around 1586, 1608, and 1645 cm^{-1}. The peaks at 1586 and 1608 cm^{-1} are assigned to the C=N stretching modes of the arginine side chain. The broad feature at 1645 cm^{-1} arises from the backbone amide C=O within the polypeptide, and its lineshape is suggestive of a disordered secondary structure with a distribution of different H-bonding environments[37]. The constituent lineshapes do not change significantly after combining AMP and Poly-R into the condensate phase. In other words, the condensate spectrum can be described as a sum of the individual components; however, there is a minor 1 cm^{-1} redshift in the high-frequency ring mode of AMP.

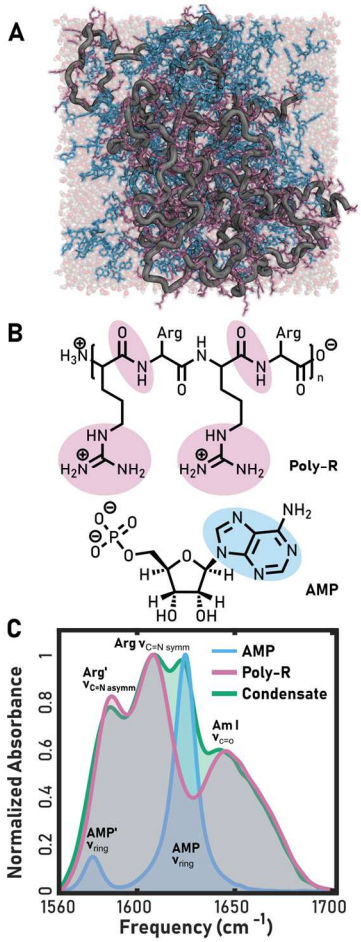

Figure 1. A. Structure of the Arginine-AMP condensate phase used in molecular dynamics simulations. The disordered peptide backbones are shown in gray, the side-chains are in red, and the AMPs are shown in blue. **B.** Chemical structures of Poly-R and AMP showing the backbone carbonyls and side-chain guanidinium groups, and the AMP ring in blue. **C.** Normalized FTIR Spectra of AMP, Poly-R, and the Poly-R and AMP combined in the condensate phase. Poly-R shows three prominent peaks centered around 1586 cm^{-1}, 1608 $cm^{-1,}$ and 1645 cm^{-1} representing the two C=N stretching, modes labeled Arg and Arg', and Amide I band, labeled Am I, composed primarily of backbone C=O stretches as indicated in the figure. AMP shows two peaks corresponding to two ring modes centered around 1577 cm^{-1} and 1624 cm^{-1} respectively.[22]

Interpretation of 2DIR Spectra.

Experimental 2D IR spectra of Poly-R, AMP, and the two components mixed in a condensate phase are shown in **Figure 2**. The peaks described in **Figure 1B** all appear as positive red peaks along the diagonal, with the corresponding negative blue peaks representing the first-to-second excited states transitions within the anharmonic vibrational modes. The Poly-R spectra show the three diagonal peaks from the FTIR 1580, 1610, and 1645 cm^{-1} representing the arginine side chain modes and the Amide I mode respectively. The AMP spectra show diagonal peaks centered at 1575 and 1625 cm^{-1} attributed to the ring modes mentioned previously, with the low-frequency mode having significantly lower intensity as seen in the FTIR. Within longer waiting

times, off-diagonal features increase in amplitude due to energy transfer. Specifically, as labeled in **Figure 2**, Poly-R and AMP spectra show off-diagonal features. These off-diagonal features represent intramolecular coupling between the 1580 cm^{-1} Arg' and 1610 cm^{-1} Arg modes and through-space coupling between the sidechain Arg', Arg, and backbone amide I modes. AMP shows off-diagonal features (**Figure 2**, AMP) due to intramolecular coupling between the AMP ring modes. Upon combining AMP and Poly-R into the condensate phase, the features observed in the individual components are all present in 2D IR spectra (**Figure 2**, Condensate), making for a convoluted spectrum. In other words, the partial overlap of the Poly-R and AMP modes and the cross peaks create highly congested spectra. Difference spectra were computed to overcome this congestion and capture the evolution of the individual component lineshapes as a function of waiting time. The difference spectra were generated by normalizing and subtracting individual component 2D IR spectra from the corresponding condensate spectra at each waiting time (**Section S2**). Difference spectra show no additional features or any cross-peaks between the AMP and Amide or Arg modes. In the case of the AMP difference spectra, there is some residual intensity from the Arg mode but it does not interfere with the analysis of the AMP mode (**Section S2**).

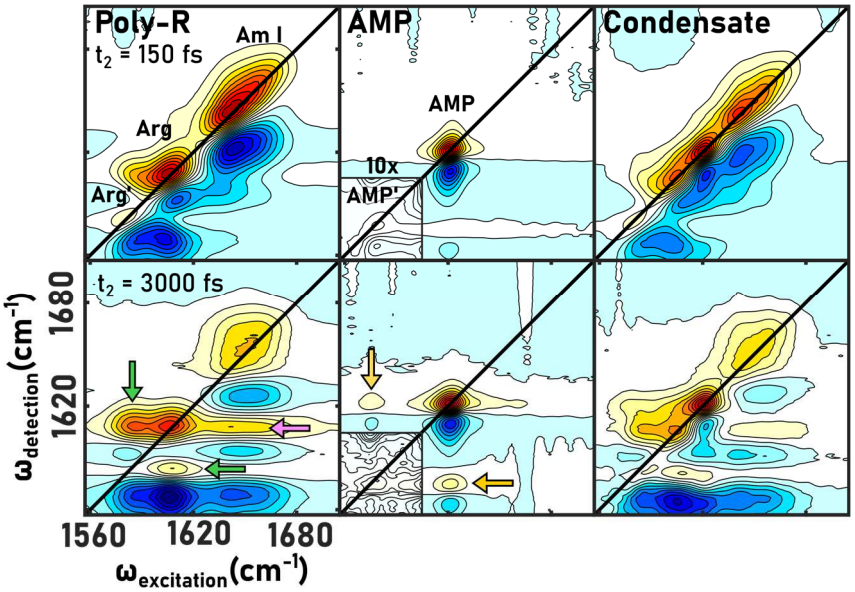

Figure 2. Measured 2D IR of Poly-R, AMP and the condensate phase formed by AMP and Poly-R at two selected waiting times, t_2 = 150 fs and t2 = 3000 fs as indicated in the panels. Along the diagonal, each spectra shows the similar features as the corresponding FTIR spectra. Cross peaks arise in the Poly-R spectra between the two Arg modes as indicated by the green arrows, as well as between the Arg and Am I modes as indicated by the purple arrow. In the AMP spectra, cross peaks appear between the two ring modes as shown by the yellow arrows. In the condensate spectra of Poly-R and AMP, the same cross peaks arise at the same locations, though the spectra become more congested compared to the individual components.

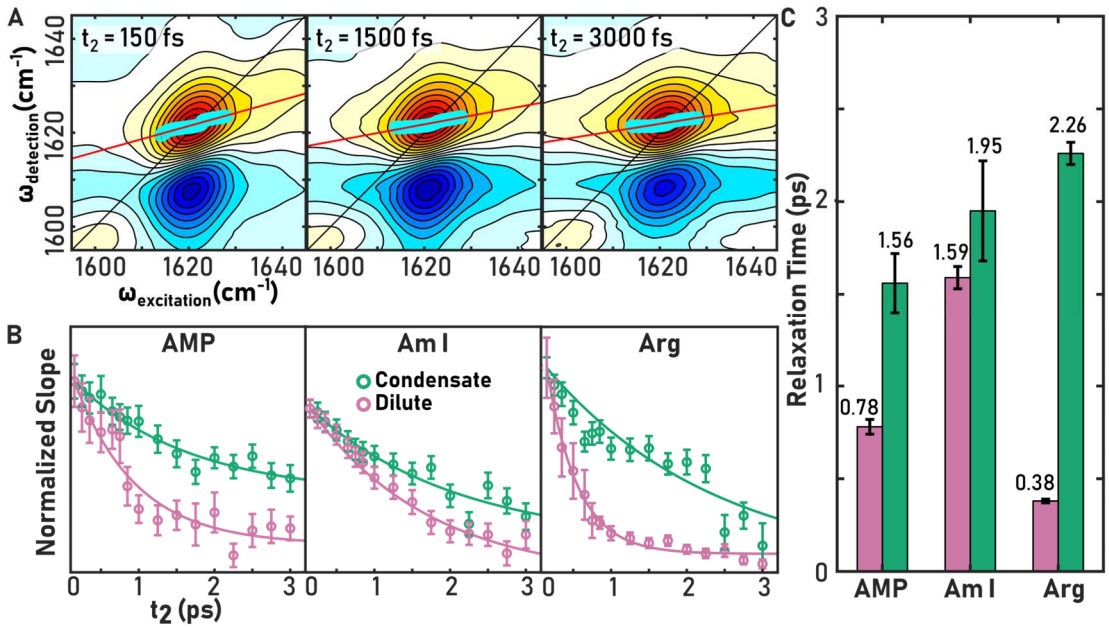

Figure 3. A. Example 2D IR spectra at three waiting times and center line slope (CLS) and linear fit analysis for the AMP ring mode (red lines). **B.** CLS relaxation as a function of the waiting time for the three diagonal lineshapes analyzed in the spectra (**Figure 1C**). The CLS values are fit to a monoexponential function with an offset. The parameters of the fit are provided in **Section S3**. **C.** Plot of the CLS exponential relaxation time (ps) for each of the three modes analyzed. The bars show that there is an overall slowdown in dynamics within the condensate phase compared to the dilute phase.

Experimental Measure of H-bond Dynamics in the Dilute and Condensate Phases.

The dynamics reported by the Arg mode, backbone carbonyl, and AMP ring were extracted through a center line slope (CLS) analysis, as illustrated in **Figure 3**. To summarize the CLS analysis process, the detection frequencies (vertical axis) corresponding to the maximum intensity along the excitation axis (horizontal axis) are selected, and a linear slope line is fit through the points. Within short excitation-detection delays, the peak is elongated along the diagonal indicating a high degree of correlation between the excitation and detection frequencies; however, as the delay is increased, reorganization of the ensembles causes randomization of the frequencies and the CLS value decreases. The change in CLS as a function of waiting time is well-represented by a monoexponential decay. This exponential represents an experimental measure of the frequency–frequency correlation function, a measure of the frequency decorrelation time. This CLS decay reports on the time evolution of the environment surrounding the vibrational probes[23,38,39]. CLS analysis was performed on each of the main 2D IR diagonal peaks corresponding to the arginine mode at 1610 cm^{-1}, the AMP ring mode at 1625 cm^{-1}, and the amide I mode around 1645 cm^{-1} and the CLS changes as a function of waiting time was fit to a monoexponential function (**Figure 3B**). Within each mode, CLS shows slower decay time constants indicating that the molecular dynamics in the condensate phase are slower than the bulk dynamics in the dilute phase. The ring and arginine modes exhibit slower dynamics around those probes and undergo a slowdown of ~2× to 6× respectively (**Figure 3C**). Smaller but different decay times around the amide I mode is also apparent, experiencing a 20% slowdown. The origin of these effects on the dynamics between the

condensate and dilute phases is interpreted through molecular dynamics simulations, as discussed in the next section.

Discussion

Local H-bond environment remains unchanged between the dilute and condensate phases.

The combination of spectroscopy and simulations provides a molecular-level view of the environments within the condensate. Measured FTIR spectra (**Figure 1**) show no significant difference in lineshapes or center frequencies for the Am I, Arg, Arg', and AMP' modes, suggesting a similar overall environment surrounding each vibrational probe. The main observation is that the AMP ring mode shows a minor ~1 cm^{-1} redshift. This shift is likely due to the strong arginine phosphate electrostatic interactions, cation-pi interactions, or a combination of these interactions[26]. However, the small changes in the spectra indicate that the environment remains largely unchanged within the condensate phase. This is consistent with previous studies suggesting that biomolecules remain hydrated within the condensate phase[40–42]. Simulations present a similar picture, the H-bond populations computed in the condensate, dilute, and single-peptide phases show no qualitative changes in the populations of the amide or arginine groups, consistent with experiment (**Figure S7**). This suggests that the strong arginine-phosphate H-bond interactions do not perturb the local environment and that water molecules can provide a substantially similar H-bonding environment.

Slowdown of dynamics within the condensate phase.

Peak shapes of the AMP ring modes in 2D IR spectra (**Figure 2**) suggest similar environments in the condensate phase. The cross peaks within the spectra are representative of intramolecular coupling within the nucleotide and have been reported previously[26]. The amide I lineshapes also indicate that the peptides remain in primarily disordered random coil configurations despite the strong electrostatic interactions and the crowded environment within the condensate phase. The change in the 2D IR lineshapes as a function of waiting time (**Figure 3A**), as captured by the CLS analysis described above, provides a direct measure of the picosecond frequency fluctuations resulting from the evolution of the local environment (**Figure 3B-C**). In general, the spectra show that dynamics slow down around each of the vibrational probes. In the amide I and arginine modes, the differences in the 2D IR dynamics are driven by fluctuations in the H-bonding environment. The amide I dynamics slows from a correlation time of 1.59 ps in the dilute phase to 1.95 ps in the condensate phase with about a 20% slowdown, showing that, overall, the dynamics are slower in the condensate phase compared to bulk water dynamics. The 20% slowdown observed is comparable to previous measurements of H-bond dynamics in crowded environments, quantifying the effect of crowders on water structure and dynamics. The similarities suggest that crowding effects may largely drive the environment around the backbone despite the strong electrostatic interactions within the condensate. On the other hand, the arginine C=N stretching modes show a significant ~6× slowdown from 0.38 ps to 2.26 ps. This is likely a result of the direct phosphate-arginine interactions that lead to long-lived H-bonds between the positive $–NH_2$ groups and the negative $–PO_4$ groups. Dynamics around the AMP ring mode were also slowed between the dilute and condensate phases from 0.78 ps to 1.56 ps respectively. Unlike the Arg and amide I modes, however, it is difficult to pinpoint the origin of this slowdown due to the inherent nature of the ring mode being delocalized across the ring structure.

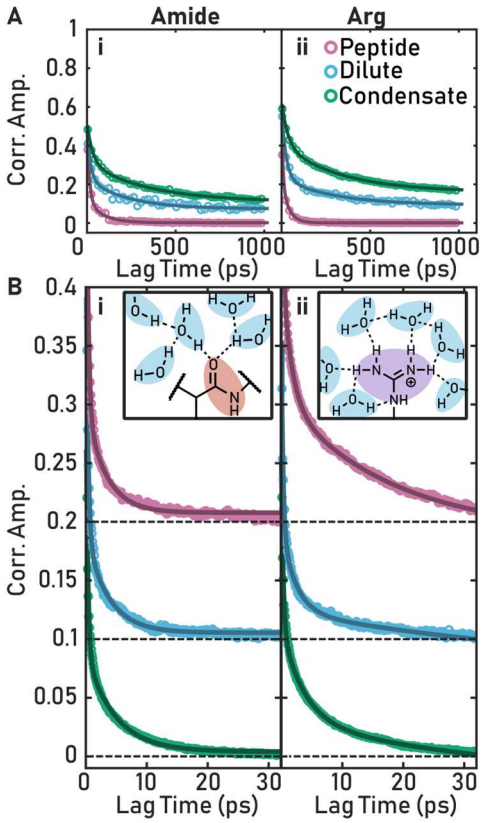

Figure 4. A. H-bond network autocorrelations for the amide backbone (i) and arginine (ii) groups extracted from MD simulations along with the exponential fits. The three systems simulated are the condensate phase (Figure 1A), a dilute phase, and the Poly-R peptide without AMP. The decays are fit to a bi-exponential. **B.** H-Bond lifetime autocorrelation. The decays are described by a biexponential (Amide (i)) or tri-exponential (Arginine (ii)) functions. Here the autocorrelations are 100 ps in length, but only the first 30 ps are shown for clarity. The fit parameters are provided in **Section S4**.

The measured 2D IR relaxation times are driven primarily by the fluctuations of the H-bond network[43]. Simulations can be used to characterize changes in H-bond dynamics between the bulk and condensate phases, which are extracted by computing the H-bond autocorrelation for each donor or acceptor group within the simulation box. Three different systems were simulated and analyzed; the condensate phase consists of 10 Poly-R 50-mer (500 arginine groups) and 250 AMP molecules for charge balance. In addition, the dilute phase is constructed as a single Poly-R peptide and 25 AMP molecules, and the Poly-R consists of a single peptide with chloride as the counter ion. The H-bond autocorrelations computed from the MD are a proxy for the local dynamics. The autocorrelations are derived from the local H-bond trajectories for each moiety. **Figure 4** shows the H-bond autocorrelations for the backbone carbonyl groups, compared to the measured amide I vibrational modes (C=O stretch) and the arginine side-chain $-NH_2$ groups, compared to the measured Arg peak (C=N stretch). The autocorrelations show a fast ~100 fs decay representing the inertial motion of the local water molecules, along with a picosecond timescale component that reports on the H-bond making and breaking timescales (i.e. the H-bond lifetime). In addition, the arginine simulations contain a long-timescale component >10 ps that can be associated with highly-

confined water molecules, as well as the overall reorganization of the H-bond network, which is analyzed in more detail below. The H-bond autocorrelations show a general slowdown in the condensate phase that agrees qualitatively with experiments. For example, the C=O H-bond lifetimes are 3.2 ps in the peptide-only simulation to 4.7 ps in the condensate, a ~38% slowdown, which compares favorably with the ~20% slowdown observed in the experiment. Similarly, the H-bond lifetimes around the arginine group undergo a 2.4× slowdown from 1.5 to 3.6 ps, in qualitative agreement with the observed ~6× slowdown in 2D IR spectroscopy. Overall, these changes suggest that the dynamics become significantly slower as a result of the crowded environment within the condensate.

In addition to the H-bond lifetimes, which report on the dynamical environment around each individual donor/acceptor within the ensemble, we compute the H-bond network identity (HNI) relaxation, which can be interpreted as an autocorrelation of the entire H-bond network. Since the identity of the donors and acceptors is considered in this analysis, the HNI accounts for fast H-bond making-breaking, similar to **Figure 4B**, but in addition, it accounts for differences between the local in-place fluctuations and diffusive reorganization of the entire H-bond network. The reorganization of the network occurs on the timescales of ~10-100 ps, significantly longer than single H-bond fluctuations and longer than timescales accessible using 2D IR spectroscopy, thus these results are purely computational. The HNI multiexponential fit results are included in **Tables S4-S5** for amide-water and arginine-water H-bond networks. The relaxation shows double-

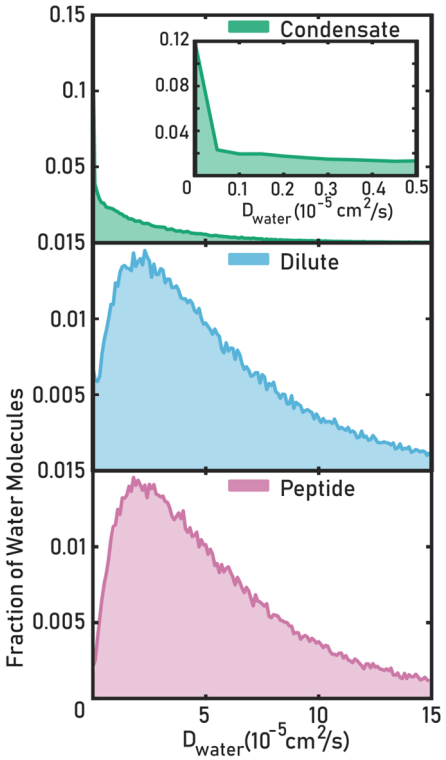

Figure 5. Histograms of the water diffusion constants extracted from a mean-squared-displacement analysis of the three systems modeled using MD simulations (see Methods section). The diffusion constants are computed from 10-ps trajectories sampled from the 100-ns production trajectory. The condensate phase shows a large fraction of "slow" water molecules, whereas the dilute and peptide-only phase show a distribution centered around 3×10^{-5} cm^2/s as is expected for bulk TIP3P water.

exponential behavior, with the short decay for arginine groups slowing from 6.3 to 35 ps and the long decay slowing from 37 to 339 ps between the bulk and the condensate simulations, respectively. The ~5-9× slowdown is consistent with the experimental 2D IR dynamics of the arginine that show ~6x slowdown within the condensate phase (**Figure 3C**), but it is important to note that the differences in timescales is because experiments report on single H-bond dynamics, not the whole H-bond network. Similarly, the amide C=O HNI slows from 12 to 31 ps for the fast component and 83 to 341 ps for the slow component. The slowdown in amide is not as pronounced as the arginine, suggesting that the strong Arginine-Phosphate interactions in the condensate phase may strongly perturb the dynamics around this group. Note that the NHI does not consider the arginine-phosphate interactions. The H-bonds between the two functional groups are "static" on the 100 ns timescale of the simulations due to the strong electrostatic interactions, giving these bonds a covalent-like character[44].

To provide further characterization of the general slowdown in dynamics within the condensate phase observed in the experiments and simulations, we compute a histogram of the diffusion coefficients extracted from short MD trajectories. These distributions (**Figure 5**) show that in the condensate phase, about 38% of the water molecules show "slow" dynamics, defined by having a diffusion constant below 1×10^{-5} cm^2/s. In contrast, in the dilute system, where only 6.4% of water molecules undergo slow diffusion, attributed to water molecules directly interacting with the peptide. This population of water with slow water diffusion agrees quite well with diffusion rates in polymer coacervates[45]. This analysis shows that the dynamics within the condensate are significantly slower overall than bulk, which explains the longer single H-bond lifetimes as well as the entire H-bond network reorganization lifetimes computed from the trajectories. Altogether, the 2D IR measurements and MD simulations are in general agreement, showing a marked slowdown within the condensate phase compared to a dilute phase.

In summary, the experiments and simulations show a general slowdown in dynamics in the condensate phase. This slowdown occurs regardless of the vibrational probe identity. We attribute these effects to the highly crowded environment within the condensate phase, resulting in a disordered water network. Although the slowdown observed in the amide is consistent with similarly crowded environments with approximately 70% water, the effects on arginine are considerably more significant[14,15,42]. This suggests that strong electrostatic interactions around these groups yield considerably slower dynamics[46]. Based on this evidence, we hypothesize that despite the strong electrostatic and cation-pi interactions, H-bond networks are primarily driven by crowding. This implies that the condensate represents a highly confined environment, which could perturb or stabilize the structures of biological molecules present within it.

Conclusion

Summary.

Our studies reveal a notable slowdown in water dynamics within peptide-nucleic acid condensates formed through liquid-liquid phase separation. We directly examined these dynamics using the amide backbone and arginine sidechain modes, as well as the nucleic acid ring mode as vibrational indicators of the local environment. MD simulations support our experimental findings, indicating 5-9× slower water dynamics as observed through H-bond lifetimes, network relaxation, and local diffusion constants. Despite strong electrostatic interactions, this slowdown may be

predominantly a result of crowding. In which crowded water behaves disordered at biomolecular interfaces and more ordered in bulk[15].

Implications for biological function.

This is a first step towards understanding the fundamental changes in the environment that stabilize the structure, folding, stability, kinetics, protein-protein, and protein-nucleic-acid interactions within biocondensates. As the localization of proteins, nucleic acids, and other biomolecules into biocondensates is becoming a more recognized aspect of biological regulation, the densely packed environment can imply significantly altered interactions as a result of dynamics[47–49]. For example, in bulk solution, the RNA backbone displays highly-heterogeneous dynamics across all temperatures and undergoes a glass-like dynamical transition involving fast hydration-shell motions that then affect the long-time scale reconfiguration[50]. Similarly, proteins undergo hydration-dependent dynamical transitions, termed "dynamic arrest"[51]. Thus, this implies that dynamical transitions may be substantially different in biocondensates as a result of the local environment, and the differences could be part of the biological regulation mechanisms. In other words, biological condensates not only recruit specific biomolecules but also control their flexibility and dynamics by altering the local environment, specifically the dynamics. Interestingly, recent studies have shown nanosecond backbone reconfiguration and diffusion of proteins slow down by approximately an order of magnitude in the condensate compared to the dilute phase, consistent with our findings of the picosecond H-bond dynamics[52]. Thus, this shows evidence that the dynamic slowdown thus propagates across several decades in time, but that bulk measurements, such as viscosity, may not be proxy for the timescales of local motions.

In conclusion, biocondensates maintain a heterogeneous but dynamic environment. The water structure may be a key factor modulating the H-bonding interactions between components[53] and may also play a role in maintaining the liquid-like properties preventing protein aggregation or rapid aging of the biomolecular condensate[54,55]. Our studies demonstrate that water behavior is significantly different in the ultra-crowded environment. The hydration shell around biomolecules remains largely intact but dynamics are slows. This study underscores the importance of examining the highly complex biocondensate microenvironments at an atomistic level over a range of timescales, including the picosecond-scale H-bond dynamics.

Materials and Methods

Sample Preparation.

Poly-L-Arginine HCl (MW: 5,000 – 15,000; Degree of Polymerization 33 - 99) and disodium adenosine 5' monophosphate (>99%) were purchased from Sigma-Aldrich. The Poly-R and AMP were lyophilized three times in D_2O to exchange protic hydrogens with deuterons to suppress background absorption in the 6 μm region of the spectrum. All experiments were done in a buffer consisting of 10 mM MOPS, 15 mM KCl, and 0.5 mM $MgCl_2$. Poly-R was combined with AMP at charge concentrations of 100 mM (1.74 mM peptide) and 50 mM (25 mM AMP), respectively to obtain the phase-separated droplets. Two additional poly-R and AMP samples were prepared separately to compare spectra in the droplet phase to the dilute phase.

Fourier Transform Infrared Spectroscopy (FTIR).

FTIR spectra were measured on a Bruker Invenio Spectrometer using a resolution of 1 cm^{-1}. In total, 25 μl of each sample was held between two 1-mm-thick CaF_2 windows with a 50 μm

spacer. Spectra were measured using a custom-built brass sample cell holder. The sample area was then purged with dry air to remove absorption from H_2O vapor signatures from the spectra. Spectra were then averaged over 64 scans with a resolution of 1 cm^{-1}. To obtain the background subtracted spectra, D_2O spectra were measured, and the spectra of interest were normalized to the OD stretch and subtracted.

Two-Dimensional Infrared Spectroscopy (2D IR).

2D IR spectra were measured using a custom-built spectrometer described in detail previously[56]. In short, the spectra were obtained by generating a sequence of three 100-fs pulses centered around 6 μm. The two excitation pulses are used to resolve the excitation frequency axis, and the detection pulse is directly measured using a dispersive spectrometer equipped with a 128x128-element MCT array. The excitation pulses are generated using a pulse shaper (PhaseTech Inc), and the excitation frequencies are generated by Fourier transforming the time delay between the two pulses. The excitation and detection pulses were in perpendicular polarization to suppress scatter. Spectra were measured at waiting times ranging from 150 fs to 3000 fs (see **Section S2**).

Molecular Dynamics Simulations.

Simulations of the condensate and dilute phases were carried out further to understand the origin of the slowdown in the experiment. Initial poly-arginine (50 units) peptide conformations were generated using the IDPConfGen software, which is designed to generate random conformations from a distribution of backbone angles extracted from the loop conformations of a random sample of PDB structures[57]. In total, 10 disordered poly-R configurations were generated as a starting point for the MD simulations. The protonation state of the peptide was chosen such that each side-chain unit carries a +1 charge for a total +50 charge for each peptide. The 10 peptide structures, along with 250 AMP molecules (–2 charge per phosphate), and 12,500 water molecules were packed randomly using the PackMol software, and, after initial packing, 125 potassium and 125 chloride ions were added using the genion GROMACS tool to approximate the ionic strength of the solutions used in experiments[58,59]. The CHARMM36 force field was used for all components as implemented in CHARMM-GUI, and the CHARMM-TIP3P model was used for water molecules[60]. The number of water molecules was chosen based on prior models of the polyelectrolyte droplet complexes, which were estimated to contain approximately 60-70% water by volume[12].

The initial conformation was energy-minimized and equilibrated in an NVT ensemble for 125 ps using the Nose-Hoover thermostat at 300 K and an integration time-step of 1 fs. The system was further equilibrated in an NPT ensemble for 100 ns using the Nose-Hoover thermostat and the Parrinello-Rahman barostat, and the integration time of 2 fs[61]. Finally, a 100 ns production trajectory was generated using the same settings as the NVT equilibration. Bonds involving hydrogen atoms were constrained using the LINCS algorithm. The equilibrated MD box configuration before the production run is shown in **Figure 1A**. Finally, snapshots saved 10 ns apart were used as a starting structure to launch ten short 1 ns simulations using the same parameters, but in which snapshots were stored every 1 ps (for HNI) or 20 fs (for H-bond lifetimes) were generated from these trajectories for further analysis. Two additional systems were constructed as a point of comparison. The first system contained a single poly-R peptide and 25 AMP, 12,500 water molecules, and 12 potassium and 12 chloride ions to represent the dilute phase. The second reference system only contained a single poly-R peptide, 50 chloride ions, and 12,500 water molecules. These additional systems were simulated using the same conditions as the condensate. All simulations were carried out using the GROMACS 2021.3 package[62–65].

The H-bond analysis was then performed using the MDAnalysis package with an H-bond donor-acceptor cutoff distance of 0.3 nm and a donor-acceptor-hydrogen cutoff angle of 150 degrees[66]. The H-bond lifetimes were subsequently computed through an autocorrelation of the H-bond trajectories of individual groups: these include the two NH2 and NH arginine groups, the individual backbone C=O groups, and the AMP phosphate group. The autocorrelations were then fit to a sum of exponentials, and the results are included in **Section S4**. In addition, an autocorrelation of the H-bond connectivity matrix, referred to as the H-bond network identity analysis, considers not only the number of H-bonds but also the identity of the donors and acceptors[67]. These autocorrelations show dynamics on timescales of ~10-300 ps, slower compared to what is accessible by 2D IR spectroscopy. The autocorrelation and fitting were done using the MATLAB R2021.b package. In addition, water diffusion constants were computed from the same short trajectories by linear fitting of the mean-squared-displacement over 10-ps windows using the built-in "msd" tool in GROMACS 2021.3.

Acknowledgments
This work was supported by the National Institutes of Health (R35GM133359), the Welch Foundation (F-1891), and the Camille and Henry Dreyfus Foundation. Simulations were carried out using the Texas Advanced Computing Center (TACC) Lonestar6 cluster. Imaging was performed at the Center for Biomedical Research Support Microscopy and Imaging Facility at UT Austin (RRID# SCR_021756).

References

(1) Banani, S. F.; Lee, H. O.; Hyman, A. A.; Rosen, M. K. Biomolecular Condensates: Organizers of Cellular Biochemistry. *Nat. Rev. Mol. Cell Biol.* **2017**, *18* (5), 285–298. https://doi.org/10.1038/nrm.2017.7.
(2) Alberti, S. Phase Separation in Biology. *Curr. Biol.* **2017**, *27* (20), R1097–R1102. https://doi.org/10.1016/j.cub.2017.08.069.
(3) *Phase Separation: Linking Cellular Compartmentalization to Disease | Elsevier Enhanced Reader*. https://doi.org/10.1016/j.tcb.2016.03.004.
(4) *Compositional Control of Phase-Separated Cellular Bodies | Elsevier Enhanced Reader*. https://doi.org/10.1016/j.cell.2016.06.010.
(5) *Considerations and Challenges in Studying Liquid-Liquid Phase Separation and Biomolecular Condensates | Elsevier Enhanced Reader*. https://doi.org/10.1016/j.cell.2018.12.035.
(6) *Protein Phase Separation: A New Phase in Cell Biology*. https://doi.org/10.1016/j.tcb.2018.02.004.
(7) Choi, J.-M.; Holehouse, A. S.; Pappu, R. V. Physical Principles Underlying the Complex Biology of Intracellular Phase Transitions. *Annu. Rev. Biophys.* **2020**, *49* (1), 107–133. https://doi.org/10.1146/annurev-biophys-121219-081629.
(8) *The role of liquid-liquid phase separation in regulating enzyme activity | Elsevier Enhanced Reader*. https://doi.org/10.1016/j.ceb.2020.12.012.
(9) Gomes, E.; Shorter, J. The Molecular Language of Membraneless Organelles. *J. Biol. Chem.* **2019**, *294* (18), 7115–7127. https://doi.org/10.1074/jbc.TM118.001192.
(10) Brangwynne, C. P.; Tompa, P.; Pappu, R. V. Polymer Physics of Intracellular Phase Transitions. *Nat. Phys.* **2015**, *11* (11), 899–904. https://doi.org/10.1038/nphys3532.

(11) Hazra, M. K.; Levy, Y. Biophysics of Phase Separation of Disordered Proteins Is Governed by Balance between Short- And Long-Range Interactions. *J. Phys. Chem. B* **2021**, *125* (9), 2202–2211. https://doi.org/10.1021/acs.jpcb.0c09975.
(12) Spruijt, E.; Westphal, A. H.; Borst, J. W.; Cohen Stuart, M. A.; van der Gucht, J. Binodal Compositions of Polyelectrolyte Complexes. *Macromolecules* **2010**, *43* (15), 6476–6484. https://doi.org/10.1021/ma101031t.
(13) Alshareedah, I.; Kaur, T.; Ngo, J.; Seppala, H.; Kounatse, L.-A. D.; Wang, W.; Moosa, M. M.; Banerjee, P. R. Interplay between Short-Range Attraction and Long-Range Repulsion Controls Reentrant Liquid Condensation of Ribonucleoprotein–RNA Complexes. *J. Am. Chem. Soc.* **2019**, *141* (37), 14593–14602. https://doi.org/10.1021/jacs.9b03689.
(14) You, X.; Baiz, C. R. Importance of Hydrogen Bonding in Crowded Environments: A Physical Chemistry Perspective. *J. Phys. Chem. A* **2022**, *126* (35), 5881–5889. https://doi.org/10.1021/acs.jpca.2c03803.
(15) *Short- and long-range crowding effects on water's hydrogen bond networks | Elsevier Enhanced Reader*. https://doi.org/10.1016/j.xcrp.2021.100419.
(16) Ribeiro, S. S.; Samanta, N.; Ebbinghaus, S.; Marcos, J. C. The Synergic Effect of Water and Biomolecules in Intracellular Phase Separation. *Nat. Rev. Chem.* **2019**, *3* (9), 552–561. https://doi.org/10.1038/s41570-019-0120-4.
(17) Ball, P. Water as an Active Constituent in Cell Biology. *Chem. Rev.* **2008**, *108* (1), 74–108. https://doi.org/10.1021/cr068037a.
(18) Bellissent-Funel, M.-C.; Hassanali, A.; Havenith, M.; Henchman, R.; Pohl, P.; Sterpone, F.; van der Spoel, D.; Xu, Y.; Garcia, A. E. Water Determines the Structure and Dynamics of Proteins. *Chem. Rev.* **2016**, *116* (13), 7673–7697. https://doi.org/10.1021/acs.chemrev.5b00664.
(19) Dahanayake, J. N.; Mitchell-Koch, K. R. Entropy Connects Water Structure and Dynamics in Protein Hydration Layer. *Phys. Chem. Chem. Phys.* **2018**, *20* (21), 14765–14777. https://doi.org/10.1039/C8CP01674G.
(20) Pappu, R. V.; Cohen, S. R.; Dar, F.; Farag, M.; Kar, M. Phase Transitions of Associative Biomacromolecules. *Chem. Rev.* **2023**, acs.chemrev.2c00814. https://doi.org/10.1021/acs.chemrev.2c00814.
(21) Ghosh, A.; Ostrander, J. S.; Zanni, M. T. Watching Proteins Wiggle: Mapping Structures with Two-Dimensional Infrared Spectroscopy. *Chem. Rev.* **2017**, *117* (16), 10726–10759. https://doi.org/10.1021/acs.chemrev.6b00582.
(22) Ganim, Z.; Chung, H. S.; Smith, A. W.; DeFlores, L. P.; Jones, K. C.; Tokmakoff, A. Amide I Two-Dimensional Infrared Spectroscopy of Proteins. *Acc. Chem. Res.* **2008**, *41* (3), 432–441. https://doi.org/10.1021/ar700188n.
(23) Park, S.; Kwak, K.; Fayer, M. D. Ultrafast 2D-IR Vibrational Echo Spectroscopy: A Probe of Molecular Dynamics. *Laser Phys. Lett.* **2007**, *4* (10), 704–718. https://doi.org/10.1002/lapl.200710046.
(24) Kim, Y. S.; Hochstrasser, R. M. Applications of 2D IR Spectroscopy to Peptides, Proteins, and Hydrogen-Bond Dynamics. *J. Phys. Chem. B* **2009**, *113* (24), 8231–8251. https://doi.org/10.1021/jp8113978.
(25) Flanagan, J. C.; Cardenas, A. E.; Baiz, C. R. Ultrafast Spectroscopy of Lipid–Water Interfaces: Transmembrane Crowding Drives H-Bond Dynamics. *J. Phys. Chem. Lett.* **2020**, *11* (10), 4093–4098. https://doi.org/10.1021/acs.jpclett.0c00783.
(26) Peng, C. S.; Jones, K. C.; Tokmakoff, A. Anharmonic Vibrational Modes of Nucleic Acid Bases Revealed by 2D IR Spectroscopy. *J. Am. Chem. Soc.* **2011**, *133* (39), 15650–15660. https://doi.org/10.1021/ja205636h.

(27) Vorobyev, D. Yu.; Kuo, C.-H.; Chen, J.-X.; Kuroda, D. G.; Scott, J. N.; Vanderkooi, J. M.; Hochstrasser, R. M. Ultrafast Vibrational Spectroscopy of a Degenerate Mode of Guanidinium Chloride. *J. Phys. Chem. B* **2009**, *113* (46), 15382–15391. https://doi.org/10.1021/jp9069256.
(28) *Tidal surge in the M2 proton channel, sensed by 2D IR spectroscopy*. https://doi.org/10.1073/pnas.1103027108.
(29) Ghosh, A.; Tucker, M. J.; Hochstrasser, R. M. Identification of Arginine Residues in Peptides by 2D-IR Echo Spectroscopy. *J. Phys. Chem. A* **2011**, *115* (34), 9731–9738. https://doi.org/10.1021/jp201794n.
(30) You, X.; Lee, E.; Xu, C.; Baiz, C. R. Molecular Mechanism of Cell Membrane Protection by Sugars: A Study of Interfacial H-Bond Networks. *J. Phys. Chem. Lett.* **2021**, *12* (39), 9602–9607. https://doi.org/10.1021/acs.jpclett.1c02451.
(31) *Site-Specific Peptide Probes Detect Buried Water in a Lipid Membrane | Elsevier Enhanced Reader*. https://doi.org/10.1016/j.bpj.2019.03.002.
(32) Edun, D. N.; Flanagan, M. R.; Serrano, A. L. Does Liquid–Liquid Phase Separation Drive Peptide Folding? *Chem. Sci.* **2021**, *12* (7), 2474–2479. https://doi.org/10.1039/D0SC04993J.
(33) Bagchi, S.; Falvo, C.; Mukamel, S.; Hochstrasser, R. M. 2D-IR Experiments and Simulations of the Coupling between Amide-I and Ionizable Side Chains in Proteins: Application to the Villin Headpiece. *J. Phys. Chem. B* **2009**, *113* (32), 11260–11273. https://doi.org/10.1021/jp900245s.
(34) Rubtsov, I. V.; Wang, J.; Hochstrasser, R. M. Vibrational Coupling between Amide-I and Amide-A Modes Revealed by Femtosecond Two Color Infrared Spectroscopy. *J. Phys. Chem. A* **2003**, *107* (18), 3384–3396. https://doi.org/10.1021/jp021922m.
(35) Kim, Y. S.; Wang, J.; Hochstrasser, R. M. Two-Dimensional Infrared Spectroscopy of the Alanine Dipeptide in Aqueous Solution. *J. Phys. Chem. B* **2005**, *109* (15), 7511–7521. https://doi.org/10.1021/jp044989d.
(36) Cakmak, F. P.; Choi, S.; Meyer, M. O.; Bevilacqua, P. C.; Keating, C. D. Prebiotically-Relevant Low Polyion Multivalency Can Improve Functionality of Membraneless Compartments. *Nat. Commun.* **2020**, *11* (1), 5949. https://doi.org/10.1038/s41467-020-19775-w.
(37) Baiz, C. R.; Peng, C. S.; Reppert, M. E.; Jones, K. C.; Tokmakoff, A. Coherent Two-Dimensional Infrared Spectroscopy: Quantitative Analysis of Protein Secondary Structure in Solution. *Analyst* **2012**, *137* (8), 1793–1799. https://doi.org/10.1039/C2AN16031E.
(38) Fayer, M. D. Dynamics of Liquids, Molecules, and Proteins Measured with Ultrafast 2D IR Vibrational Echo Chemical Exchange Spectroscopy. *Annu. Rev. Phys. Chem.* **2009**, *60* (1), 21–38. https://doi.org/10.1146/annurev-physchem-073108-112712.
(39) Kwak, K.; Rosenfeld, D. E.; Fayer, M. D. Taking Apart the Two-Dimensional Infrared Vibrational Echo Spectra: More Information and Elimination of Distortions. *J. Chem. Phys.* **2008**, *128* (20), 204505. https://doi.org/10.1063/1.2927906.
(40) Ahlers, J.; Adams, E. M.; Bader, V.; Pezzotti, S.; Winklhofer, K. F.; Tatzelt, J.; Havenith, M. The Key Role of Solvent in Condensation: Mapping Water in Liquid-Liquid Phase-Separated FUS. *Biophys. J.* **2021**, *120* (7), 1266–1275. https://doi.org/10.1016/j.bpj.2021.01.019.
(41) Wei, M.-T.; Elbaum-Garfinkle, S.; Holehouse, A. S.; Chen, C. C.-H.; Feric, M.; Arnold, C. B.; Priestley, R. D.; Pappu, R. V.; Brangwynne, C. P. Phase Behaviour of Disordered Proteins Underlying Low Density and High Permeability of Liquid Organelles. *Nat. Chem.* **2017**, *9* (11), 1118–1125. https://doi.org/10.1038/nchem.2803.

(42) Choi, S.; Chun, S. Y.; Kwak, K.; Cho, M. Micro-Raman Spectroscopic Analysis of Liquid–Liquid Phase Separation. *Phys. Chem. Chem. Phys.* **2023**, 10.1039.D2CP05115J. https://doi.org/10.1039/D2CP05115J.
(43) Kolano, C.; Helbing, J.; Kozinski, M.; Sander, W.; Hamm, P. Watching Hydrogen-Bond Dynamics in a β-Turn by Transient Two-Dimensional Infrared Spectroscopy. *Nature* **2006**, *444* (7118), 469–472. https://doi.org/10.1038/nature05352.
(44) Woods, A. S.; Ferré, S. Amazing Stability of the Arginine−Phosphate Electrostatic Interaction. *J. Proteome Res.* **2005**, *4* (4), 1397–1402. https://doi.org/10.1021/pr050077s.
(45) Kausik, R.; Srivastava, A.; Korevaar, P. A.; Stucky, G.; Waite, J. H.; Han, S. Local Water Dynamics in Coacervated Polyelectrolytes Monitored through Dynamic Nuclear Polarization-Enhanced 1H NMR. *Macromolecules* **2009**, *42* (19), 7404–7412. https://doi.org/10.1021/ma901137g.
(46) Schug, K. A.; Lindner, W. Noncovalent Binding between Guanidinium and Anionic Groups: Focus on Biological- and Synthetic-Based Arginine/Guanidinium Interactions with Phosph[on]Ate and Sulf[on]Ate Residues. *Chem. Rev.* **2005**, *105* (1), 67–114. https://doi.org/10.1021/cr040603j.
(47) Bonucci, A.; Palomino-Schätzlein, M.; Malo de Molina, P.; Arbe, A.; Pierattelli, R.; Rizzuti, B.; Iovanna, J. L.; Neira, J. L. Crowding Effects on the Structure and Dynamics of the Intrinsically Disordered Nuclear Chromatin Protein NUPR1. *Front. Mol. Biosci.* **2021**, *8*.
(48) Feig, M.; Yu, I.; Wang, P.; Nawrocki, G.; Sugita, Y. Crowding in Cellular Environments at an Atomistic Level from Computer Simulations. *J. Phys. Chem. B* **2017**, *121* (34), 8009–8025. https://doi.org/10.1021/acs.jpcb.7b03570.
(49) Elcock, A. H. Models of Macromolecular Crowding Effects and the Need for Quantitative Comparisons with Experiment. *Curr. Opin. Struct. Biol.* **2010**, *20* (2), 196–206. https://doi.org/10.1016/j.sbi.2010.01.008.
(50) Yoon, J.; Lin, J.-C.; Hyeon, C.; Thirumalai, D. Dynamical Transition and Heterogeneous Hydration Dynamics in RNA. *J. Phys. Chem. B* **2014**, *118* (28), 7910–7919. https://doi.org/10.1021/jp500643u.
(51) Caliskan, G.; Briber, R. M.; Thirumalai, D.; Garcia-Sakai, V.; Woodson, S. A.; Sokolov, A. P. Dynamic Transition in TRNA Is Solvent Induced. *J. Am. Chem. Soc.* **2006**, *128* (1), 32–33. https://doi.org/10.1021/ja056444i.
(52) Galvanetto, N.; Ivanović, M. T.; Chowdhury, A.; Sottini, A.; Nüesch, M. F.; Nettels, D.; Best, R. B.; Schuler, B. *Ultrafast Molecular Dynamics Observed within a Dense Protein Condensate*; preprint; Biophysics, 2022. https://doi.org/10.1101/2022.12.12.520135.
(53) Zaslavsky, B. Yu.; Bagirov, T. O.; Borovskaya, A. A.; Gulaeva, N. D.; Miheeva, L. H.; Mahmudov, A. U.; Rodnikova, M. N. Structure of Water as a Key Factor of Phase Separation in Aqueous Mixtures of Two Nonionic Polymers. *Polymer* **1989**, *30* (11), 2104–2111. https://doi.org/10.1016/0032-3861(89)90301-7.
(54) *A Liquid-to-Solid Phase Transition of the ALS Protein FUS Accelerated by Disease Mutation*. https://doi.org/10.1016/j.cell.2015.07.047.
(55) Wang, B.; Zhang, L.; Dai, T.; Qin, Z.; Lu, H.; Zhang, L.; Zhou, F. Liquid–Liquid Phase Separation in Human Health and Diseases. *Signal Transduct. Target. Ther.* **2021**, *6* (1), 1–16. https://doi.org/10.1038/s41392-021-00678-1.
(56) *Coordination to lanthanide ions distorts binding site conformation in calmodulin*. https://doi.org/10.1073/pnas.1722042115.
(57) Teixeira, J. M. C.; Liu, Z. H.; Namini, A.; Li, J.; Vernon, R. M.; Krzeminski, M.; Shamandy, A. A.; Zhang, O.; Haghighatlari, M.; Yu, L.; Head-Gordon, T.; Forman-Kay, J. D. IDPConformerGenerator: A Flexible Software Suite for Sampling the Conformational

Space of Disordered Protein States. *J. Phys. Chem. A* **2022**, *126* (35), 5985–6003. https://doi.org/10.1021/acs.jpca.2c03726.
(58) Martínez, L.; Andrade, R.; Birgin, E. G.; Martínez, J. M. PACKMOL: A package for building initial configurations for molecular dynamics simulations. *J. Comput. Chem.* **2009**, *30* (13), 2157–2164. https://doi.org/10.1002/jcc.21224.
(59) Martínez, J. M.; Martínez, L. Packing Optimization for Automated Generation of Complex System's Initial Configurations for Molecular Dynamics and Docking. *J. Comput. Chem.* **2003**, *24* (7), 819–825. https://doi.org/10.1002/jcc.10216.
(60) Jo, S.; Kim, T.; Iyer, V. G.; Im, W. CHARMM-GUI: A Web-Based Graphical User Interface for CHARMM. *J. Comput. Chem.* **2008**, *29* (11), 1859–1865. https://doi.org/10.1002/jcc.20945.
(61) Cheng, A.; Merz, K. M. Application of the Nosé−Hoover Chain Algorithm to the Study of Protein Dynamics. *J. Phys. Chem.* **1996**, *100* (5), 1927–1937. https://doi.org/10.1021/jp951968y.
(62) Berendsen, H. J. C.; van der Spoel, D.; van Drunen, R. GROMACS: A Message-Passing Parallel Molecular Dynamics Implementation. *Comput. Phys. Commun.* **1995**, *91* (1), 43–56. https://doi.org/10.1016/0010-4655(95)00042-E.
(63) Páll, S.; Zhmurov, A.; Bauer, P.; Abraham, M.; Lundborg, M.; Gray, A.; Hess, B.; Lindahl, E. Heterogeneous Parallelization and Acceleration of Molecular Dynamics Simulations in GROMACS. *J. Chem. Phys.* **2020**, *153* (13), 134110. https://doi.org/10.1063/5.0018516.
(64) Van Der Spoel, D.; Lindahl, E.; Hess, B.; Groenhof, G.; Mark, A. E.; Berendsen, H. J. C. GROMACS: Fast, Flexible, and Free. *J. Comput. Chem.* **2005**, *26* (16), 1701–1718. https://doi.org/10.1002/jcc.20291.
(65) Lindahl, E.; Hess, B.; van der Spoel, D. GROMACS 3.0: A Package for Molecular Simulation and Trajectory Analysis. *Mol. Model. Annu.* **2001**, *7* (8), 306–317. https://doi.org/10.1007/s008940100045.
(66) Michaud-Agrawal, N.; Denning, E. J.; Woolf, T. B.; Beckstein, O. MDAnalysis: A Toolkit for the Analysis of Molecular Dynamics Simulations. *J. Comput. Chem.* **2011**, *32* (10), 2319–2327. https://doi.org/10.1002/jcc.21787.
(67) Oh, K.-I.; You, X.; Flanagan, J. C.; Baiz, C. R. Liquid–Liquid Phase Separation Produces Fast H-Bond Dynamics in DMSO–Water Mixtures. *J. Phys. Chem. Lett.* **2020**, *11* (5), 1903–1908. https://doi.org/10.1021/acs.jpclett.0c00378.